

The anatomical location shapes the immune infiltrate in tumors of same etiology and impacts survival

Saskia J.A.M. Santegoets¹, Vanessa J. van Ham¹, Ilina Ehsan¹, Pornpimol Charoentong², Chantal L. Duurland¹, Vincent van Unen³, Thomas Höllt^{4,5}, Lilly-Ann van der Velden^{6,7}, Sylvia L. van Egmond⁶, Kim E. Kortekaas⁸, Peggy J. de Vos van Steenwijk⁸, Mariëtte I.E. van Poelgeest⁸, Marij J.P. Welters¹, Sjoerd H. van der Burg¹.

Departments of ¹Medical Oncology, ³Immunohematology and Blood Transfusion, ⁴Computational Biology Center, ⁶Otorhinolaryngology and Head and Neck Surgery, and ⁸Gynaecology, Leiden University Medical Center, Leiden, The Netherlands. ²Department of Medical Oncology, National Center for Tumor Diseases, University of Heidelberg, Germany. ⁵Computer Graphics and Visualization Group, Delft University of Technology, Delft, The Netherlands. ⁷Current address, Department of Head and Neck Oncology and Surgery, Netherlands Cancer Institute-Antoni van Leeuwenhoek, Amsterdam, the Netherlands.

Running title: The tissue of origin shapes the TME and impacts survival

Abbreviation list: BLCL: B-lymphoblastoid cell lines; CxCa: cervical carcinoma; CyTOF: high-dimensional single-cell mass cytometry; FFPE: formalin-fixed paraffin-embedded; HPV: human papillomavirus; ICS: intracellular cytokine staining; IHC: immunohistochemistry; MIATA: Minimal Information About T-cell Assays; NGS: next-generation sequencing; OPSCC: oropharyngeal squamous cell carcinoma; PBMC: peripheral blood mononuclear cells; SLP: synthetic long peptide; Tcm: central memory T-cell; TDLN: tumor draining lymph node; Teff: effector T-cell; Tem: effector memory T-cell; Temra: effector memory RA+ T-cells; Th1: T helper

1; TIL: tumor infiltrating lymphocyte; Tn: naïve T-cell; 2D-PCA: 2-dimensional principal component analysis.

Keywords: mass cytometry, tumor microenvironment, HPV, anatomical location, CD161

Corresponding author: S.H. van der Burg, Department of Medical Oncology, Albinusdreef 2, 2233 ZA Leiden, the Netherlands. Phone: +31 71 5261180, Email: shvdburg@lumc.nl.

Conflict of interest: The authors have no conflicting financial interests.

Funding: This study was financially supported by grants from the Dutch Cancer Society 2014-6696 to SHvdB, LAvdV and MJW and 2016-10726 to SHvdB, MJW and SJAMS.

Text word count: 4867 words (excluding references and legends)

Abstract word count: 161 words

Number of Figures and Tables: 7 Figures

Number of References: 44 references

Supplementary: 5 Figures and 3 Tables.

Translational relevance

The tumor immune contexture determines therapy responsiveness and survival. It develops as a consequence of the interaction between the tumor cells and the host. While there is accumulating evidence on the contribution of tumor intrinsic factors, the impact of the

tissue microenvironment in which the tumor develops is largely unknown. Our study of the immune cell populations present in human papillomavirus-induced primary tumors of the cervix and oropharynx, two tumors that share the same virus-driven oncogenic pathway but arise in different anatomical locations, allowed us to address this question. We show that the microenvironment of the original tissue has an influence on the constitution of the intratumoral lymphocytic infiltrate, the efficiency of tumor-specific T cells to infiltrate the tumor, and as such the response and survival of patients after therapy. These results will fuel the discussion on therapeutic approaches aiming to treat tumors driven by common oncogenic pathways.

Abstract

Purpose: The tumor immune microenvironment determines clinical outcome. Whether the original tissue in which a primary tumor develops influences this microenvironment is not well understood.

Experimental Design: We applied high-dimensional single-cell mass cytometry (CyTOF) analysis and functional studies to analyze immune cell populations in human papillomavirus (HPV)-induced primary tumors of the cervix (CxCa) and oropharynx (OPSCC).

Results: Despite the same etiology of these tumors, the composition and functionality of their lymphocytic infiltrate substantially differed. CxCa displayed a 3-fold lower CD4:CD8 ratio, contained more activated CD8+CD103+CD161+ effector T-cells and less CD4+CD161+ effector memory T-cells than OPSCC. CD161+ effector cells produced the highest cytokine levels among tumor-specific T-cells. Differences in CD4+ T-cell infiltration between CxCa and OPSCC were reflected in the detection rate of intratumoral HPV-specific CD4+ T-cells and in their impact on OPSCC and CxCa survival. The PBMC composition of these patients, however, was similar.

Conclusions: The tissue of origin significantly impacts the overall shape of the immune infiltrate in primary tumors.

Introduction

The tumor microenvironment is involved in tumorigenesis and tumor progression (1). Analyses of many tumor types revealed that a strong T helper 1 (Th1) cytotoxic microenvironment is associated with a more favorable prognosis and therapy responsiveness (2,3). When the tumor metastasizes to other anatomical locations the original immune contexture of the primary tumor is maintained (4), indicating that the immune contexture of the primary tumor determines the therapy response of later metastases (5). However, whether the microenvironment of the original tissue in which the primary tumor arises has an impact on the shape of the tumor microenvironment, has largely been neglected. Perhaps because primary tumors of the same type can have different mutations and activated oncogenic pathways, some of which are known to impact the constitution of the tumor microenvironment. For instance, overexpression of BRAF, loss of PTEN and activation of the WNT/ β -catenin signaling pathway modulate the extent of the lymphocytic tumor infiltrate (6-8). In this context it is hard to dissect the potential influence of the original tissue on the tumor microenvironment. An answer to what extent the immune contexture can be imprinted by the site or origin may come from studies on human papillomavirus (HPV) induced tumors. Although these tumors can arise in different anatomical locations (cervix, vagina, vulva, anus and oropharynx), they share the same virus-driven oncogenic pathway.

HPV is strictly epitheliotropic and infects basal epithelial cells in skin and mucous membranes. Integration of the viral genome into the host DNA leads to overexpression of the E6 and E7 oncoproteins and finally to transformation of the epithelial basal cells into cancer cells (9). Within the cervix, the cells close to the squamo-columnar junction, in what is called the transformation zone, are susceptible to HPV infection, transformation and progression to cancer (10). Notably, within the genital tract it is the normal uterine cervix, including the transformation zone that contains the highest numbers of immune cells (11,12). The oropharynx comprises the palatine tonsils, the soft palate, the tongue base and the posterior pharyngeal wall, but HPV almost exclusively infects and transforms the highly specialized lympho-epithelium lining the tonsillar crypts (13). A direct comparison of the lymphocytic infiltrate in routinely removed non-diseased fresh tonsils and cervical tissue revealed differences in the CD4:CD8 T-cell ratio and the distribution of central memory

(Tcm) and effector memory (Tem) CD4⁺ T-cells between the two tissue types (14). The indication that these two issues at different anatomical locations already display a different immune contexture under non-cancerous conditions provides an opportunity to assess if the original tissue microenvironment also bears impact on the tumor immune microenvironment.

To study the potential impact of the original tissue on the intratumoral immune contexture we analyzed immune cell populations in a series of primary tumors, tumor draining lymph nodes (TDLN) and peripheral blood mononuclear cell (PBMC) samples, obtained from patients with either HPV-driven cervical carcinoma (CxCa) or oropharyngeal squamous cell carcinoma (OPSCC), by high-dimensional single-cell mass cytometry (CyTOF) and different functional analyses, including the assessment of HPV-specific T-cells. Our data shows that primary tumors of the same etiology, but arising in different anatomical locations, are infiltrated with distinct lymphocytic populations, and that the anatomical location affects the efficiency of tumor-specific T-cells to infiltrate the tumor.

Materials and methods

The authors acknowledge the reporting of Minimal Information About T-cell Assays (MIATA).

Patients

Patients included in this study were part of two larger observational studies on CxCa and OPSCC. Women with histologically proven cervical carcinoma (International Federation of Gynecology and Obstetrics 1a2, 1b1/2) were included in the CIRCLE study investigating cellular immunity against anogenital lesions (15,16). Patients with histology-confirmed OPSCC were included in the P07-112 study investigating the circulating and local immune response in patients with head and neck cancer (17,18). Patients were included after signing informed consent. Both studies were conducted in accordance with the Declaration of Helsinki and approved by the local medical ethical committee of the Leiden University Medical Center (LUMC) and in agreement with the Dutch law. The patients received standard-of-care treatment consisting of surgery, radiotherapy, chemotherapy, treatment

with monoclonal antibody or combinations hereof. HPV typing and p16^{ink4a} IHC staining was performed on formalin-fixed paraffin-embedded (FFPE) tumor sections at the LUMC Department of Pathology as described (19). Tumor staging was done according to the National Comprehensive Cancer Network (<https://www.nccn.org/professionals>). An overview of patient characteristics and treatment is given in Table SI.

TP53 mutational status OPSCC tumors

We performed an immunohistochemistry (IHC) staining for p53 on the tissue sections of the OPSCC tumors as described previously (20). An experienced pathologist reviewed all slides and scored the specimen as “wild-type” (p53wt) when nuclei of the tumor cells stained weak to moderately, comparable with adjacent normal epithelium.

In addition, next-generation sequencing (NGS) was performed as described previously (21). In brief, formalin-fixed paraffin-embedded tissue blocks of the OPSCC tumors were micro-dissected to get a tumor percentage of >70%. Tumor DNA was isolated using the Tissue Preparation System with VERSANT Tissue Preparation Reagents, (Siemens Healthcare Diagnostics, Tarrytown, NY), after which somatic variant analysis of the *TP53* gene was performed using the AmpliSeq Cancer Hotspot Panel 4 (ThermoFisher Scientific) with a sequence coverage of 90 %. Results of this analysis are shown in table 1.

Blood, LN and tumor cell isolation and culturing

Venous blood samples were drawn prior to surgery, and peripheral blood mononuclear cells (PBMC) were isolated using Ficoll density gradient centrifugation as described previously (18,22). CxCa and OPSCC tumor and CxCa TDLN material or biopsies were obtained and handled as described (16,18). First, tumor material was cut into small pieces. One-third of the tumor pieces were incubated for 60 minutes at 37°C in Iscove’s Modified Dulbecco’s Medium (IMDM, Lonza, Verviers, Belgium) with 10% human AB serum (Capricorn Scientific, Esdorfergrund, Germany) and supplemented with high dose of antibiotics (50 µg/ml Gentamycin (Gibco/ Thermo Fisher Scientific (TFS), Bleiswijk, the Netherlands), 25 µg/ml Fungizone (Invitrogen/TFS), 100 IU/ml penicillin (pen; Gibco/TFS) and 100 µg/ml streptomycin (strep; Gibco/TFS)), after which the tumor pieces were put in culture in IMDM supplemented with 10% human AB serum, 100 IU/ml penicillin, 100 µg/ml streptomycin, 2 mM L-glutamin (Lonza, Breda, Netherlands; IMDM complete) and 1000 IU/ml human

recombinant IL-2 (Aldesleukin, Novartis, Arnhem, the Netherlands). Cultures were replenished every 2-3 days with fresh IMDM complete and IL-2 to a final concentration of 1000 IU/ml. When there were sufficient T-cells, the cells were cryopreserved and stored in liquid nitrogen until use. Approximately two-third of the tumor pieces were incubated for 30 minutes at 37°C in IMDM dissociation mixture containing 10% human AB serum, high dose of antibiotics (as above) and 50 µg/ml DNase I (Roche, Woerden, the Netherlands), and 1 mg/ml collagenase D (Roche), after which the tumor was dispersed to single cells using the GentleMACS dissociator (Miltenyi) with a company-installed program (h_tumor_02). Following centrifugation, cells were resuspended in PBS (B. Braun, Melsungen, Germany), put on a 70 µm cell strainer (Falcon, Durham, NC, USA) to obtain a single cell suspension, counted using trypan blue exclusion (Sigma, St Louis, MO, USA), and cryopreserved at approximately 2 million cells/vial. All tumor samples from OPSCC and part of the CxCa samples were dissociated as above. From patient C1016 onwards, the approach to prepare single cell suspensions was adjusted. The DNase I/collagenase D enzymes were replaced by 0.38 mg/ml of the commercially available Liberase enzymes (Liberase TL, research grade, Roche), the incubation period was reduced to 15 minutes, and the GentleMACS dissociator was no longer used.

Single cell suspensions from CxCa TDLN material were prepared either through DNase I and collagenase D dissociation as described above with or without the use of the GentleMACS dissociator, or by scraping the cutting surface of the LN with a surgical scalpel blade, after which they were cryopreserved until further analysis. To generate TDLN-derived T-cell batches, ex vivo TDLN were expanded as described previously (22). In brief, ex vivo TDLN were thawed, washed and seeded at a density of 0.4–1 × 10⁶ cells per well in a 24-well plate in 1 ml of IMDM complete medium and stimulated with 5 µg/ml HPV16 E6 and E7 clinical grade long peptide pools in the presence of 150 U/ml recombinant human IL-2. Cultures were replenished every 2-3 days with fresh IMDM complete and IL-2 and after 22-28 days the expanded T-cells were cryopreserved and stored in the vapor phase of liquid nitrogen until further use.

Mass cytometry analysis

Blood and matched tumor and/or LN samples from 20 CxCa and nine OPSCC patients were analyzed by mass cytometry (CyTOF). Details on antibodies used are listed in Table S2.

Conjugation of the purified antibodies with the isotopic tags was done using the MaxPar X8 antibody labeling kit (Fluidigm Sciences) according to manufacturer's instructions and following conjugation the antibodies were stored at 4°C in Candor PBS Antibody Stabilization Buffer (Candor Bioscience GmbH). Mass cytometry antibody staining and acquisition procedures were performed as described (REF v Unen Immunity). In brief, cell samples were thawed according to standard operation procedures and stained with 1 µM Cell-ID intercalator-103Rh (Fluidigm Sciences) for 15 minutes at room temperature (RT) to identify dead cells. Following incubation, the cells were washed with MaxPar Cell stain buffer (Fluidigm Sciences), and incubated with Human TruStain FcX Fc Receptor Blocking Solution (Biolegend) for at least 10 minutes at RT. Next, cells were incubated with the metal-conjugated antibodies for 45 minutes at RT. After the cells were washed twice with the MaxPar Cell stain buffer, the cells were stained overnight at 4°C with 125 nM Cell-ID intercalator-Ir in MaxPar Fix and Perm Buffer (Fluidigm Sciences). The next day, cells were washed and acquired by CyTOF 2 or helios-upgraded CyTOF2 mass cytometer (Fluidigm Sciences). Data were normalized by using EQ Four Element Calibration Beads (Fluidigm Sciences) with the reference EQ passport P13H2302.

Mass cytometry data analysis

Gating for single, live CD45+ cells for each PBMC, LN or tumor sample was done using the cloud-based Cytobank software (Fluidigm Sciences; example in supplementary Fig. S1). The high-dimensional single cell data was analyzed by analysis by tSNE analysis in Cytosplore with default parameters (perplexity, 30; iterations, 1,000) (23) and by the fully automated hierarchical clustering (unsupervised) tool CITRUS using the cytobank software. The different cell populations were visualized and quantified.

Tumor-specific T-cell reactivity analysis

To determine the specificity of T-cells infiltrating the tumor and/or TDLN, cultured TIL and TDLN T-cell batches from HPV16+ CxCa and OPSCC tumors were analyzed for the presence of HPV16-specific T-cells using 5-days [3H]-thymidine-based proliferation assay as described (18). T-cell responses against autologous HPV16 E6/E7 synthetic long peptide (SLP; 22-mers with 14 amino acids overlap) loaded monocytes were tested in triplicate. PHA (0.5 µg/ml; HA16 Remel; ThermoFischer Scientific) was taken along as positive control, while unloaded

monocytes served as negative control. At day 1.5 and 4 supernatant (50 μ l/well) was harvested to determine cytokine production. During the last 16 h of culture, 0.5 μ Ci/well of [3H]thymidine was added to measure proliferation. The stimulation index was calculated as the average of test wells divided by the average of the medium control wells. A positive response was defined as a stimulation index of at least 3.

Antigen-specific cytokine production was determined by cytometric bead array (Th1/Th2 kit, BD Bioscience, Breda, the Netherlands) according to the manufacturer's instructions. The cutoff value for cytokine production was 20 pg/ml, except for IFN γ for which it was 100 pg/ml. Positive cytokine production was defined as at least twice above that of the unstimulated cells.

The HPV16-reactivity of TIL was also determined by intracellular cytokine (ICS) staining. Intracellular cytokine staining (ICS) for the markers CD3, CD4, CD8, CD137, CD154, CD161, CD103, IFN γ and TNF α was performed as described previously (18) following stimulation with HPV16 E6/E7 SLP-loaded autologous monocytes or EBV-transformed B-lymphoblastoid cell lines (BLCL). Unloaded autologous monocytes or BLCL cells were used as negative and Staphylococcal Enterotoxin B (SEB; 2 μ g/mL; Sigma) was used as positive control. A positive response was defined as at least twice the value of the negative control and at least 10 events in the gate. Acquisition of cells was done on a LSRII Fortessa (BD Biosciences). Data was analysed using DIVA software (version 6.2 or 8.02 BD Biosciences).

Statistical analysis

Non-parametric (Wilcoxon signed-rank or Mann–Whitney test for two samples and Friedman or Kruskal–Wallis with Dunn's multiple comparison test for multiple samples) and parametric (paired or unpaired *t* test for two samples or RM one-way ANOVA or ordinary one-way ANOVA with Tukey's multiple comparison test for multiple samples) tests were performed as appropriate. For survival analysis, patients were grouped into two groups according to the median (i.e., grouped into below or above the median of the total group for each parameter), after which survival was tested using Kaplan–Meier method, and statistical significance of the survival distribution was analyzed by log-rank testing. All statistical tests were performed at the 0.05 significance level, and differences were considered significant when $p < 0.05$, as indicated with an asterisk ($\#p < 0.1$, $*p < 0.05$, $**p < 0.01$, $*** p < 0.001$

and **** $p < 0.0001$). Statistical analyses were performed using GraphPad Prism 7.1 (San Diego, USA).

Results

Cervical tumors but not TDLN are highly infiltrated by CD8+CD103+ T-cells.

First, the lymphocyte content was studied in a series of tumors, TDLN and PBMC samples of patients with HPV-induced primary CxCa (supplementary Table S1) using 36-parameter mass cytometry (Table S2). tSNE analyses of all samples revealed different clusters of B cells, NK cells and several populations of CD4+ and CD8+ T-cells (Fig. 1A and B and supplementary Fig. S1). Clearly, the naïve (Tn), Tcm and Tem populations of CD4+ and the Tcm/Tem populations of CD8+ T-cells did not differ between PBMC and LN (Fig. 1C). In contrast, the tumor showed a strong enrichment of CD8+ T-cells, which were mainly effector T-cells (Teff; Fig. 1B and C). Further analysis of the tSNE populations revealed eight distinctive (groups of) lymphocyte populations (Fig. 1D), and demonstrated that CxCa TDLN contained more total B cells (both IgM- and IgM+ B cells) while more NK cells were found in PBMC (Fig. 1D). Strikingly, the percentage of total CD4+ T-cells was lower in tumors, albeit that those of CD4+ Treg-like cells was higher. CD8+ T-cells were enriched in tumors, in particular the CD8+CD103+ T-cells, also known as long-lived tissue-resident memory cells (24). Thus, while the T-cell populations in CxCa TDLN more or less resembled that of PBMC, CxCa tumors displayed a more prominent CD8+CD103+ T-cell infiltrate, with the CD8+ T-cells in ratio of about 1:1 to CD4+ T-cells.

The populations of tumor-infiltrating lymphocytes differ between CxCa and OPSCC.

Next, the lymphocyte content of the CxCa samples was compared to a series of tumor and blood samples from patients with HPV-induced OPSCC. 2D principal component analysis (2D-PCA; Fig 2A) revealed clear phenotypic diversity between tumor, TDLN and PBMC samples as well as between the groups of CxCa and OPSCC tumor samples (Fig. 2A). Combined tSNE analysis of paired blood and tumor samples resulted in the identification of 29 distinct immune populations (Fig. 2, B and C). Subsequent comparison of the immune cell content showed that the lymphocytic composition of CxCa and OPSCC greatly differed with

respect to the percentages of IgM+ B cells, CD4+ T-cells and CD8+ T-cells (Fig. 2D). The lymphocytic composition of PBMC samples was quite similar for CxCa and OPSCC (Fig. 2E). In order to automatically discover stratifying biological signatures within the OPSCC and CxCa blood and tumor samples, we made use of the automated and data-driven CITRUS platform, as an unbiased and thorough correlation-based tool for mining and inspection of cell subsets nested within high-dimensional datasets (25). The CITRUS analysis resulted in 30 distinctive (groups of) lymphocyte populations (Fig. 3A and B, and supplementary Fig. S2 and Table S3). Closer inspection of the types of lymphocytes in CxCa and OPSCC revealed that the percentage of IgM+ B cells is higher in OPSCC and comprised two different populations (subsets 3 and 4; Fig 3C) that differed with respect to surface levels of CD27 and HLA-DR (supplementary Fig. S2). Major differences were observed with respect to infiltrating T-cells (Fig. 3E and F and supplementary Fig. S2 and Table S3). This was not biased by the higher frequency of B cells in OPSCC, as similar differences were also observed within the total CD3+ T-cell population (supplementary Fig. S3A, B). CxCa displayed a slightly lower infiltration with CD8+ Tcm/Tem (subset 15) and a more dense infiltration of CD8+ effector memory RA+ T-cells (Temra; subset 17). In addition, CxCa were highly infiltrated with CD8+CD103+CD161- Teff (subsets 8 and 11) and CD8+CD103+CD161+ Teff (subsets 9 and 10) cells. Subset 8 Teff cells (CD27-HLADR-CD38dimPD1-) seem less activated based on their profile. A fifth population of CD8+CD103+ Teff (subset 12) and a population of CD8+ Teff, expressing intermediate levels of CD103, HLA-DR, CD27, CD38 and PD-1 (subset 14) were more prominent in OPSCC. At the CD4+ T-cell level, OPSCC contained more CD4+ Tn (subsets 19-21) and potentially CD4+CD161+ Tcm (subset 28). Levels of CD4+CD161+ Tem (subsets 22-24) were clearly higher in OPSCC and comprised populations of CD27+ and CD27- cells. We also observed two populations of CD4+ cells with a Treg-like phenotype (subsets 26 and 27) but their levels were similar in CxCa and OPSCC. Notably, there were no gross differences in the composition of CD8+ and CD4+ T-cells in the blood of CxCa and OPSCC patients.

Thus, HPV-driven CxCa and OPSCC differ considerably with respect to their lymphocytic infiltrate. In OPSCC, more intratumoral IgM+ B cells as well as CD4+ Tn and CD4+CD161+ Tem were found, while CxCa contained higher numbers of CD8+CD103+ Teff and in particular CD8+CD103+CD161+ cells. Importantly, lymph node involvement or absence

thereof in cervical cancer did not account for these observed differences between the CxCa and OPSCC tumor immune environment (supplementary Fig. S3C, D).

CD161 identifies tumor-specific T-cells with the strongest effector function.

Since the large majority of CD8+CD103+ Tem and CD4+ Tem co-expressed CD161 we next examined their functional properties. To this end, tumor infiltrating lymphocyte (TIL) cultures containing HPV-specific T-cells were stimulated with cognate antigen and cytokine production was analyzed in CD103 and CD161 double negative, single positive and double positive CD4 (n=28) or CD8 (n=9) responding T-cell populations (Fig. 4A-C). CD8 reactivity was predominantly found in CD103+CD161+ and CD103+CD161- T-cells, with more than half of the responding CD8+ T-cells expressing CD161. About 40% of the cytokine producing CD4+ T-cells expressed CD161 (Fig. 4B and C). Moreover, the expression of CD103 and/or CD161 within the CD4+ and CD8+ T-cell populations is not biased by changes in their expression following antigenic stimulation, as CD103 and CD161 expression was shown stable following HPV16 and SEB stimulation (supplementary Fig. S4). Importantly, the level of cytokine production – based on the mean fluorescence intensity of cytokine staining (26,27) – was higher in CD161+ CD4+ or CD8+ T-cells (Fig. 4A and D), suggesting that CD161+ T-cells are highly activated. To substantiate this notion, the staining intensity of surface markers expressed by CD161+ and CD161- CD4+ and CD8+ T-cells infiltrating CxCa and OPSCC tumors was analyzed (Fig. 4E). In both types of tumors, CD4+CD161+ T-cells expressed higher levels of CD103, PD-1 and CD127, while levels of CD25, CD27 and CD45RA were lower. CD8+CD161+ T-cells displayed higher levels of CD103, HLA-DR and PD-1, whereas levels of CD45RA and CCR7 were lower (Fig. 4E). Collectively, this classifies CD4+CD161+ and CD8+CD103+CD161+ TIL as highly activated effector T-cells.

The general lymphocyte composition of primary tumors is comparable to the tissue of origin.

A recent publication on flow cytometric analyses of the percentages of CD4+ and CD8+ subpopulations in routinely removed non-diseased fresh tonsils and cervical tissue (14) prompted us to compare this with the composition of these populations in OPSCC and CxCa. Interestingly, the CD4:CD8 ratios in CxCa tumors resembled that of normal cervical epithelium, while the CD4:CD8 ratio in CxCa TDLN and OPSCC were more similar to normal tonsil (Fig. 5A). These data are consistent with our calculations showing that the median

CD4:CD8 tumor-infiltrating T-cell ratio in CxCa is not different from normal cervical epithelium (0.41 vs 0.51, respectively) as measured by immunohistochemistry (28) and is 3 fold lower than the CD4:CD8 ratio (1.56) in OPSCC (29). Furthermore, the composition of CD8+ Tn, Tcm, Tem and Temra within CxCa and CxCa TDLN showed similarity to normal cervical tissue and tonsils, respectively. This was not the case for OPSCC and normal tonsils (Fig. 5B). The composition of CD4+ T-cells was different in OPSCC and CxCa compared to normal tissue (Fig. 5C). The CD4+ and CD8+ T-cell populations in CxCa TDLN paralleled that of PBMC (Fig. 5B and C). Thus, CxCa and OPSCC strongly differ with respect to the composition of CD8+ and CD4+ T-cell subsets and CD4:CD8 ratio, the latter of which is more comparable to the tissue of origin. The observation that the CD4:CD8 ratio and composition of CD4 and CD8 Tn, Tcm, Tem, and Temra of HPV-driven OPSCC is similar to that of OPSCC with a non-viral etiology (supplementary Fig. S5) also suggests an impact of the location on the tumor immune microenvironment.

Tumor-specific CD4+ T-cells were more often found in OPSCC and CxCa TDLN than CxCa.

To determine whether the differences in CD4+ T-cell infiltration between CxCa and OPSCC were also visible at the tumor-specific T-cell level, we compared the detection rate of HPV16-specific CD4+ T-cell responses in CxCa (n=48), TDLN of CxCa (n=18) and OPSCC (n=53) as analyzed and reported by us earlier (15-18,22). Indeed, HPV16-specific T-cell reactivity significantly differed between the groups and was detected in 35% of CxCa, 100% of CxCa TDLN, and 63% of OPSCC (Fig. 6). The detection of HPV16-specific CD4+ T-cells in all CxCa TDLN, including those of patients in which the matched TIL samples did not show reactivity (n=2), and in only 35% of HPV16+ CxCa tumors suggest that the infiltration of CxCa by tumor-specific CD4+ T-cells is hampered.

Differences in CD4+ T-cell infiltration are reflected in survival of OPSCC and CxCa patients.

Previously, we showed that a strong infiltration with CD4+ T-cells and CD4+CD161+ T-cells is positively associated with survival in patients with HPV+ OPSCC (18). Consequently, the lower CD4+ T-cell infiltration observed in CxCa would predict that here CD4+ T-cell infiltration would have less impact on clinical outcome. First, we analyzed the effect of CD4 gene expression in a group of 214 squamous CxCa patients within the publicly available cancer genomic atlas (TCGA) database (30). Patients with higher than median CD4

expression in CxCa tumors displayed no survival benefit (Fig. 7A), irrespective of molecular classification as CD4⁺ T_{cm} or T_{em} (31). In addition, we performed follow-up analysis of a group of 38 CxCa patients from whom we had previously analyzed the tumors with respect to T-cell infiltration by immunohistochemistry (19). This analysis confirmed that there is no significant impact on survival when the patients were divided based on the median number of tumor-infiltrating CD4⁺ T-cells in CxCa (Fig. 7B). Thus, the number of CD4⁺ T-cells is generally lower in CxCa than OPSCC and this is reflected by a different impact on survival of CD4⁺ T-cells in these two tumor types.

Detection of HPV-specific T-cells in OPSCC is a strong predictor for patient survival in OPSCC (18). Hence, we analyzed the value of this in patients with CxCa from whom we cultured TIL and were able to test HPV-specificity. In contrast to a group of 51 OPSCC patients, the detection of HPV-specific T-cells among ex-vivo expanded TIL was not able to predict survival in a set of 42 CxCa patients (Fig. 7C and D). Most likely, because the total CD4⁺ T-cell number and thus also that of HPV-specific T-cells – before the in vitro expansion - is too low to mediate any strong effect in vivo. Interestingly, whenever an HPV-specific CD4⁺ T-cell response was detected in the tumor, the percentage of CD4⁺CD161⁺ T_{em} were higher in both OPSCC and CxCa (Fig. 7E). As we showed that the intratumoral CD4⁺CD161⁺ T-cell population is highly activated, we assessed whether high numbers of CD4⁺CD161⁺ effector cells would have the same positive association with survival in CxCa as previously reported by us for OPSCC (18). Indeed, the group of CxCa patients with high expression levels of CD4 and CD161 in the tumor showed a better outcome (Fig. 7F).

Discussion

We exploited the fact that HPV16 can cause tumors to arise in different tissues to study the extent to which the anatomical location contributes to the immune contexture of a developing primary tumor. Application of our high-dimensional single-cell mass cytometry-based approach with 36 markers in freshly digested tumor samples and PBMC of patients with CxCa or OPSCC identified 30 distinctive clusters of lymphocytes. These findings are the first line of evidence showing that tumors of the same etiology, but arising in a different tissue, have a different immune contexture. In a direct comparison, OPSCC contained more B cells and showed a specific enrichment with subpopulations of CD4⁺CD161⁺ T_{em} whereas several subpopulations of CD8⁺CD103⁺ T_{eff} were enriched in CxCa. In addition, the CD4:CD8

ratio was 3-fold higher in OPSCC than CxCa. Finally, HPV-specific TIL were more frequently detected in OPSCC than CxCa.

Interestingly, the CD4:CD8 ratio in OPSCC closely resembled the ratio found in normal tonsils (14) and the CD4:CD8 ratio in CxCa is highly similar to that found in normal cervical epithelium as measured by flow cytometry (14,32) and immunohistochemistry (11,12,28). Furthermore, the percentages of CD8⁺ T_n, T_{cm}, T_{em} and T_{emra} found in CxCa are comparable to previous reported findings in normal cervical tissue (14). Moreover, the numbers of CxCa resident (CD8⁺CD103⁺) T cells display the same mean and variability as found in normal cervix (33), suggesting that these cells are already present in normal tissue and thus not appear due to malignant transformation. It seems that the different immune contexts developed in primary OPSCC and CxCa reflect the immune contexture found in the tissue of origin. This notion is sustained by the observation that OPSCC of non-viral etiology display a similar general (CD4:CD8 ratio and percentages of T_n, T_{cm}, T_{em} and T_{emra}) immune infiltration as HPV-driven OPSCC. Evidently, differences in the distribution of naïve and effector memory CD4⁺ and CD8⁺ T-cells between healthy tonsil (and TDLN) and cervical tissue is explained by the fact that tonsil and TDLN are secondary lymphoid organs where naïve T cells recirculate (34).

In contrast to CD8⁺ T-cells, the composition of the CD4⁺ T-cell population in OPSCC and CxCa was different from healthy tissue. A strong infiltration of OPSCC with CD4⁺ T-cells was found to be beneficial for survival in three independent cohorts and this was correlated to their functional activity, as indicated by strong expression of HLA-DR, CD38 and PD-1 (35) with or without CD161 and by expression of Tbet (18). Activated CD4⁺ T_{eff} cells producing IFN γ and TNF α were shown to induce permanent growth arrest in the Simian virus 40 large T antigen driven β -cancer cell model (36,37). CD4⁺ T-cells were also responsible for control of spontaneous cervical tumor outgrowth in genetically engineered K14-HPV16 transgenic mice. Within this model, a strong reduction of progressive precursor lesions was found when the HPV-specific CD4⁺ T-cell levels and activity were boosted by vaccination (38). Hence, tumor-specific CD4⁺ T-cells actively participate in tumor control. However, here we showed that the relative CD4⁺ T-cell numbers are lower in CxCa than OPSCC. In addition, comparison of median CD4⁺ T-cell infiltration numbers in two previous studies in CxCa and one in OPSCC performed with similar techniques (18,19,28) showed that the absolute median number of CD4⁺ T-cell infiltration per square millimeter of tumor was 2-fold lower

in CxCa than OPSCC. Moreover, this difference was also reflected in their association with patient's survival. While division of OPSCC patients based on their median infiltration with CD4+ T-cells showed a beneficial clinical effect, this was not observed in CxCa patients. Similar to our previous findings in OPSCC (18), CD4+ T-cell mediated survival benefit is found for CxCa patients with high levels of highly active CD4+ T-cells, which are identified by CD161. Moreover, CD161+ Teff produced the highest amounts of type 1 cytokines upon activation with their cognate tumor antigen. Intermediate expression (as compared to MAIT cells) of CD161 has identified CD4+ and CD8+ mucosal Teff and Tcm cells as highly functional type 1/17 cytokine producing cell (39-43). Acute GVHD is associated with high CD4+CD161+ to CD8+CD161+ ratio (44) validating a role in tissue rejection specifically for the CD4+ T-cell population. However, high levels of CD4 and CD161 were only observed in a small group of CxCa patients. The numerical and relative lower abundance of CD4+ T-cells in CxCa, which is also observed in normal cervical tissue, suggests that the lack of sufficient attraction of CD4+ T-cells is intrinsic to the location. This notion is sustained by our observation that in all patients tested, HPV-specific CD4+ T-cell responses are detected in the TDLN. However, HPV-specific CD4+ T-cells were only found in a minor fraction of the large set of CxCa patients analyzed.

Thus, the strong differences in lymphocytic infiltrate between oncogenic HPV-driven primary CxCa and OPSCC indicate a role for the originating tissue in shaping the immune contexture. Our results imply that the problem of CD4+ T-cell attraction in CxCa will continue to exist throughout the progression of disease and suggests that it should form a point of focus for future immunotherapeutic approaches aiming to treat progressive CxCa.

Acknowledgements

We thank the patients for participating in this study.

References

1. Witz IP. The tumor microenvironment: the making of a paradigm. *Cancer Microenviron* **2009**;2 Suppl 1:9-17.
2. Galon J, Angell HK, Bedognetti D, Marincola FM. The continuum of cancer immunosurveillance: prognostic, predictive, and mechanistic signatures. *Immunity* **2013**;39:11-26.
3. Fridman WH, Pages F, Sautes-Fridman C, Galon J. The immune contexture in human tumours: impact on clinical outcome. *Nat Rev Cancer* **2012**;12:298-306.
4. Remark R, Alifano M, Cremer I, Lupo A, Dieu-Nosjean MC, Riquet M, *et al.* Characteristics and clinical impacts of the immune environments in colorectal and renal cell carcinoma lung metastases: influence of tumor origin. *Clinical cancer research : an official journal of the American Association for Cancer Research* **2013**;19:4079-91.
5. Giraldo NA, Becht E, Remark R, Damotte D, Sautes-Fridman C, Fridman WH. The immune contexture of primary and metastatic human tumours. *Curr Opin Immunol* **2014**;27:8-15.
6. Liu C, Peng W, Xu C, Lou Y, Zhang M, Wargo JA, *et al.* BRAF inhibition increases tumor infiltration by T cells and enhances the antitumor activity of adoptive immunotherapy in mice. *Clinical cancer research : an official journal of the American Association for Cancer Research* **2013**;19:393-403.
7. Peng W, Chen JQ, Liu C, Malu S, Creasy C, Tetzlaff MT, *et al.* Loss of PTEN Promotes Resistance to T Cell-Mediated Immunotherapy. *Cancer Discov* **2016**;6:202-16.
8. Spranger S, Bao R, Gajewski TF. Melanoma-intrinsic beta-catenin signalling prevents anti-tumour immunity. *Nature* **2015**;523:231-5.

9. zur Hausen H. Papillomaviruses and cancer: from basic studies to clinical application. *Nat Rev Cancer* **2002**;2:342-50.
10. Doorbar J, Quint W, Banks L, Bravo IG, Stoler M, Broker TR, *et al.* The biology and life-cycle of human papillomaviruses. *Vaccine* **2012**;30 Suppl 5:F55-70.
11. Pudney J, Quayle AJ, Anderson DJ. Immunological microenvironments in the human vagina and cervix: mediators of cellular immunity are concentrated in the cervical transformation zone. *Biol Reprod* **2005**;73:1253-63.
12. Poppe WA, Drijkoningen M, Ide PS, Lauweryns JM, Van Assche FA. Lymphocytes and dendritic cells in the normal uterine cervix. An immunohistochemical study. *Eur J Obstet Gynecol Reprod Biol* **1998**;81:277-82.
13. Gelwan E, Malm IJ, Khararjian A, Fakhry C, Bishop JA, Westra WH. Nonuniform Distribution of High-risk Human Papillomavirus in Squamous Cell Carcinomas of the Oropharynx: Rethinking the Anatomic Boundaries of Oral and Oropharyngeal Carcinoma From an Oncologic HPV Perspective. *Am J Surg Pathol* **2017**;41:1722-8.
14. Saba E, Grivel JC, Vanpouille C, Brichacek B, Fitzgerald W, Margolis L, *et al.* HIV-1 sexual transmission: early events of HIV-1 infection of human cervico-vaginal tissue in an optimized ex vivo model. *Mucosal Immunol* **2010**;3:280-90.
15. de Vos van Steenwijk PJ, Heusinkveld M, Ramwadhoebe TH, Lowik MJ, van der Hulst JM, Goedemans R, *et al.* An unexpectedly large polyclonal repertoire of HPV-specific T cells is poised for action in patients with cervical cancer. *Cancer Res* **2010**;70:2707-17.
16. Piersma SJ, Welters MJ, van der Hulst JM, Kloth JN, Kwappenberg KM, Trimbos BJ, *et al.* Human papilloma virus specific T cells infiltrating cervical cancer and draining

- lymph nodes show remarkably frequent use of HLA-DQ and -DP as a restriction element. *Int J Cancer* **2008**;122:486-94.
17. Heusinkveld M, Goedemans R, Briet RJ, Gelderblom H, Nortier JW, Gorter A, *et al.* Systemic and local human papillomavirus 16-specific T-cell immunity in patients with head and neck cancer. *Int J Cancer* **2012**;131:E74-85.
 18. Welters MJP, Ma W, Santegoets S, Goedemans R, Ehsan I, Jordanova ES, *et al.* Intratumoral HPV16-Specific T Cells Constitute a Type I-Oriented Tumor Microenvironment to Improve Survival in HPV16-Driven Oropharyngeal Cancer. *Clinical cancer research : an official journal of the American Association for Cancer Research* **2018**;24:634-47.
 19. Piersma SJ, Jordanova ES, van Poelgeest MI, Kwappenberg KM, van der Hulst JM, Drijfhout JW, *et al.* High number of intraepithelial CD8+ tumor-infiltrating lymphocytes is associated with the absence of lymph node metastases in patients with large early-stage cervical cancer. *Cancer Res* **2007**;67:354-61.
 20. Nooij LS, Ter Haar NT, Ruano D, Rakislova N, van Wezel T, Smit V, *et al.* Genomic Characterization of Vulvar (Pre)cancers Identifies Distinct Molecular Subtypes with Prognostic Significance. *Clinical cancer research : an official journal of the American Association for Cancer Research* **2017**;23:6781-9.
 21. Ten Broeke SW, van Bavel TC, Jansen AML, Gomez-Garcia E, Hes FJ, van Hest LP, *et al.* Molecular Background of Colorectal Tumors From Patients With Lynch Syndrome Associated With Germline Variants in PMS2. *Gastroenterology* **2018**.
 22. van Poelgeest MI, Visconti VV, Aghai Z, van Ham VJ, Heusinkveld M, Zandvliet ML, *et al.* Potential use of lymph node-derived HPV-specific T cells for adoptive cell therapy of cervical cancer. *Cancer Immunol Immunother* **2016**;65:1451-63.

23. Höllt T, Pezzotti N, van Unen V, Koning F, Eisemann E, Lelieveldt B, *et al.* Cytosplore: Interactive Immune Cell Phenotyping for Large Single-Cell Datasets. *Computer Graphics Forum* **2016**;35:171-80.
24. Topham DJ, Reilly EC. Tissue-Resident Memory CD8(+) T Cells: From Phenotype to Function. *Front Immunol* **2018**;9:515.
25. Bruggner RV, Bodenmiller B, Dill DL, Tibshirani RJ, Nolan GP. Automated identification of stratifying signatures in cellular subpopulations. *Proc Natl Acad Sci U S A* **2014**;111:E2770-7.
26. Darrah PA, Hegde ST, Patel DT, Lindsay RW, Chen L, Roederer M, *et al.* IL-10 production differentially influences the magnitude, quality, and protective capacity of Th1 responses depending on the vaccine platform. *J Exp Med* **2010**;207:1421-33.
27. Darrah PA, Patel DT, De Luca PM, Lindsay RW, Davey DF, Flynn BJ, *et al.* Multifunctional TH1 cells define a correlate of vaccine-mediated protection against *Leishmania major*. *Nat Med* **2007**;13:843-50.
28. Jordanova ES, Gorter A, Ayachi O, Prins F, Durrant LG, Kenter GG, *et al.* Human leukocyte antigen class I, MHC class I chain-related molecule A, and CD8+/regulatory T-cell ratio: which variable determines survival of cervical cancer patients? *Clinical cancer research : an official journal of the American Association for Cancer Research* **2008**;14:2028-35.
29. Wansom D, Light E, Thomas D, Worden F, Prince M, Urba S, *et al.* Infiltrating lymphocytes and human papillomavirus-16--associated oropharyngeal cancer. *Laryngoscope* **2012**;122:121-7.

30. Comprehensive genomic characterization of head and neck squamous cell carcinomas. Cancer Genome Atlas Network. 2015/01/30 ed. Volume 5172015. p 576-82.
31. Charoentong P, Finotello F, Angelova M, Mayer C, Efremova M, Rieder D, *et al.* Pan-cancer Immunogenomic Analyses Reveal Genotype-Immunophenotype Relationships and Predictors of Response to Checkpoint Blockade. *Cell Rep* **2017**;18:248-62.
32. Trifonova RT, Lieberman J, van Baarle D. Distribution of immune cells in the human cervix and implications for HIV transmission. *Am J Reprod Immunol* **2014**;71:252-64.
33. Rodriguez-Garcia M, Fortier JM, Barr FD, Wira CR. Aging impacts CD103(+) CD8(+) T cell presence and induction by dendritic cells in the genital tract. *Aging Cell* **2018**;e12733.
34. Butcher EC, Picker LJ. Lymphocyte homing and homeostasis. *Science* **1996**;272:60-6.
35. Badoual C, Hans S, Merillon N, Van Ryswick C, Ravel P, Benhamouda N, *et al.* PD-1-expressing tumor-infiltrating T cells are a favorable prognostic biomarker in HPV-associated head and neck cancer. *Cancer Res* **2013**;73:128-38.
36. Braumuller H, Wieder T, Brenner E, Assmann S, Hahn M, Alkhaled M, *et al.* T-helper-1-cell cytokines drive cancer into senescence. *Nature* **2013**;494:361-5.
37. Wieder T, Braumuller H, Brenner E, Zender L, Rocken M. Changing T-cell enigma: cancer killing or cancer control? *Cell Cycle* **2013**;12:3146-53.
38. Daniel D, Chiu C, Giraudo E, Inoue M, Mizzen LA, Chu NR, *et al.* CD4+ T cell-mediated antigen-specific immunotherapy in a mouse model of cervical cancer. *Cancer Res* **2005**;65:2018-25.

39. Cohavy O, Shih DQ, Doherty TM, Ware CF, Targan SR. CD161 defines effector T cells that express LIGHT and respond to TL1A-DR3 signaling. *Eur J Microbiol Immunol (Bp)* **2011**;1:70-9.
40. Fergusson JR, Huhn MH, Swadling L, Walker LJ, Kurioka A, Llibre A, *et al.* CD161(int)CD8+ T cells: a novel population of highly functional, memory CD8+ T cells enriched within the gut. *Mucosal Immunol* **2016**;9:401-13.
41. Gonzalez Y, Herrera MT, Juarez E, Salazar-Lezama MA, Bobadilla K, Torres M. CD161 Expression Defines a Th1/Th17 Polyfunctional Subset of Resident Memory T Lymphocytes in Bronchoalveolar Cells. *PLoS One* **2015**;10:e0123591.
42. Takahashi T, Dejbakhsh-Jones S, Strober S. Expression of CD161 (NKR-P1A) defines subsets of human CD4 and CD8 T cells with different functional activities. *J Immunol* **2006**;176:211-6.
43. Duurland CL, Brown CC, O'Shaughnessy RF, Wedderburn LR. CD161(+) Tconv and CD161(+) Treg Share a Transcriptional and Functional Phenotype despite Limited Overlap in TCRbeta Repertoire. *Front Immunol* **2017**;8:103.
44. Lee SE, Lim JY, Yoon JH, Shin SH, Cho BS, Eom KS, *et al.* CD161(+) T cells as predictive markers for acute graft-versus-host disease. *Biol Blood Marrow Transplant* **2015**;21:421-8.

Figure legend

Figure 1. HPV-induced cervical carcinoma (CxCa) tumors are highly infiltrated by CD8+CD103+ effector T-cells. Peripheral blood mononuclear cells (PBMC), tumor draining lymph nodes (TDLN) and tumors of CxCa patients were analyzed by 36-parameter mass cytometry analysis. **(A)** A tSNE density plot (left) and corresponding cluster partitions (right) visualizing the high-dimensional CyTOF data in two dimensions for the collective immune cells derived from 20 CxCa patients' PBMC, TDLN and tumors (n=19, n=12 and n=9 patients, respectively). The identified cell subsets are indicated in the plots by numbers, and groups of B cells, myeloid cells, NK cells and CD4+ and CD8+ T-cells are specified by different colors. **(B)** Pie charts showing the composition and relative contribution of the immune cells in CxCa PBMC (left), TDLN (middle) and tumor (right). **(C)** The subdivision of the CD4+ and CD8+ T-cell frequencies (mean \pm SEM) into naïve (Tn; CCR7+CD45RA+CD127-), central memory (Tcm; CCR7+CD45RA-CD127+) and effector memory (Tem; CCR7-CD45RA-CD127+) T-cells for CD4 (left; orange) or into Tn, Tcm/em, effector (Teff; CCR7-CD45RA-CD127-) and CD45RA+ effector memory T-cells (Temra; CCR7-CD45RA+CD127-) for CD8 (right; pink). Significant differences in the effector/memory distribution of CD4+ and CD8+ T-cells between PBMC, TDLN and tumors were found. **(D)** Box and whiskers (plus min-max) plots depicting eight distinctive (groups of) lymphocyte populations within CxCa PBMC, TDLN and tumor samples. * p <0.05; ** p <0.01, *** p <0.001 and **** p <0.0001.

Figure 2. CxCa and OPSCC tumors show different populations of infiltrating lymphocytes. PBMC, TDLN and tumor samples from HPV-induced CxCa and OPSCC patients were analyzed by combined tSNE analysis. **(A)** 2-dimensional principal component analysis (2D-PCA) depicting the collective t-SNE dimensionality reduced cell percentage data (as percentage of CD45⁺ cells) of 30 subsets for 63 samples (n=28, n=17 and n=18 for PBMC, TDLN and tumor samples, respectively). Every dot represents a single sample. The color and shape of the sample shows the corresponding clinical information (CxCa versus OPSCC and tumor versus TDLN versus PBMC). **(B)** A tSNE density plot (left) and corresponding cluster partitions (right) of collective total CD45+ immune cells of 35 samples (n=9 for CxCa and OPSCC tumor, n=9 and n=8 for CxCa and OPSCC PBMC). The identified cell subsets are indicated in the plots by

numbers, and groups of B cells, myeloid cells, NK cells and CD4+ and CD8+ T-cells are specified by different colors. **(C)** Heatmap visualizing the 29 identified cell clusters for the collective total CD45+ immune cells derived from 35 samples. Shown are ArcSinh5-transformed values of marker expression (green to pink scale) and hierarchical clustering of markers and subsets. The groups of NK cells, myeloid cells, B cells, CD4+ and CD8+ T-cells are indicated underneath the map. **(D and E, top)** tSNE density plots of collective CxCa (left) and OPSCC (right) total CD45+ immune cells of **(D)** 18 tumor samples (n=9 for CxCa and OPSCC patients) and **(E)** 17 PBMC samples (n=9 for CxCa and n=8 for OPSCC patients). **(D and E, bottom)** Pie charts showing composition and relative contribution of the identified immune cell subsets in CxCa (left; purple) and OPSCC (right; green) in tumor **(D)** and PBMC **(E)**.

Figure 3. Clustering analysis using CITRUS revealed 30 distinctive populations of B cells, NK cells and T-cells. Automatic discovery of stratifying biological signatures within tumor and blood samples was performed using the CITRUS algorithm to identify significantly different cell populations in 35 tumor and PBMC samples (n=9 for CxCa and OPSCC tumor and n=9 and n=8 for CxCa and OPSCC PBMC). Every cell population represented by a node is divided on basis of median level of expression into two new nodes (cellular subsets) going from the center (all cells) to the periphery of the plot. **(A and B)** CITRUS analysis visualizing **(A)** six distinctive populations of B and NK cells within the total CD45+ immune population and **(B)** 24 distinctive populations of CD8+ and CD4+ T-cells within the total CD3+ immune population. The parental (total CD45 or total CD3) nodes are depicted in black. The total CD45 node divides into total T-cell (depicted in red) and non-T-cell nodes with B cell (blue), NK cell (pink) and myeloid cell (orange) nodes. The total CD3 node divides into CD8+ T-cell (depicted in pink) and CD4+ T-cell (depicted in orange) nodes. **(C-F)** Box and whiskers (plus min-max) plots displaying frequencies of **(C)** B cells (subsets 1 to 4), **(D)** NK cells (subset 5 and 6), **(E)** CD8+ T-cells (subsets 7-18) and **(F)** CD4+ T-cells (subsets 19-30) as % of lymphocytes for CxCa (purple) and OPSCC (green) tumors and PBMC. #p<0.1, *p<0.05, **p<0.01, ***p<0.001 and ****p<0.0001.

Figure 4. CD161 identifies HPV16-specific CD4⁺ and CD8⁺ T-cells with the strongest effector function. Three CxCa and three OPSCC TIL cultures containing HPV-specific T-cells (as determined by [3H]-thymidine-based proliferation assay) were selected and analyzed for HPV16-reactivity by intracellular cytokine (ICS) staining following stimulation with pools of HPV16 E6/E7 synthetic long peptides (SLPs) or protein-loaded autologous monocytes or BLCL. Expression of CD3, CD4, CD8, CD137, CD154, CD161, CD103, IFN γ and TNF α following overnight stimulation in the presence of Brefeldin A was determined by flow cytometry. (A) A representative example of an HPV16-reactive CD4⁺ and CD8⁺ T-cell response within TIL of an OPSCC patient is shown. The TIL were first gated for viable and single cells, and further gated for CD3, CD4 and CD8. Within the CD4⁺ (top) and CD8⁺ (bottom) T-cell population, the cells expressing CD103 and/or CD161 were gated and IFN γ and TNF α is depicted. The red dotted lines indicates the mean TNF α signal observed in CD103-CD161⁻ cells. (B and C) The distribution of the different cell populations within the total cytokine-producing HPV-specific population (i.e. IFN γ +TNF α ⁻, IFN γ +TNF α ⁺ and IFN γ -TNF α ⁺ cells) is shown for CD4⁺ (left) and CD8⁺ (right) T-cells in TIL of (B) a representative OPSCC patient and (C) for all 28 CD4⁺ T-cell and nine CD8 T-cell mediated responses detected in all six HPV16-reactive CxCa and OPSCC patients. (D) The mean fluorescence intensity of TNF α and IFN γ within the CD103-CD161⁻, CD103+CD161⁻, CD103+CD161⁺ and CD103-CD161⁺ populations is depicted for CD4⁺ T-cells and CD8⁺ T-cells. (E) Expression ratio of CD161⁺ versus CD161⁻ CD4⁺ and CD8⁺ T-cells for each marker for nine CxCa (purple) and nine OPSCC (green) tumors is given on a log₁₀ scale. Each symbol represents an individual tumor sample. Markers with an increased expression ratios within CD4⁺ or CD8⁺ T-cells are indicated with an arrow. * p <0.05; ** p <0.01, *** p <0.001 and **** p <0.0001.

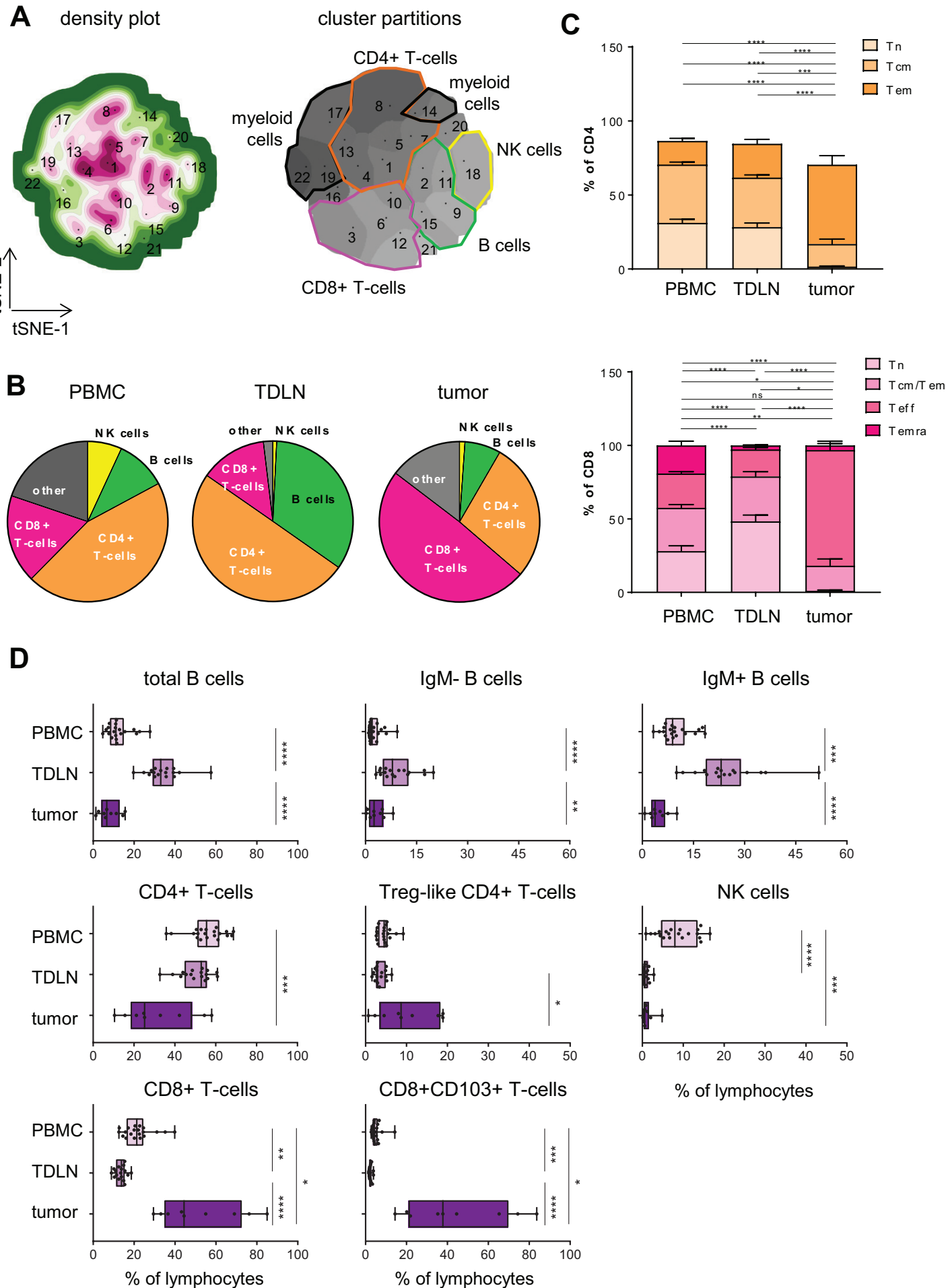
Figure 5. CD4:CD8 ratios in CxCa and OPSCC tumors resemble those found in the original tissue. Frequencies of CD4 and CD8 T-cells, and effector/memory distribution (based on CD45RA and CCR7 expression) within these populations, were determined in TDLN and/or PBMC and tumor samples of CxCa and OPSCC samples by mass cytometry after manual gating. CD4:CD8 ratios, and effector/memory distribution within CD4⁺ and CD8⁺ T-cells of normal cervical epithelium and healthy tonsils, measured by flow cytometry, were obtained from Saba and co-workers (14). (A) Bar graphs depicting the CD4:CD8 ratio in the indicated

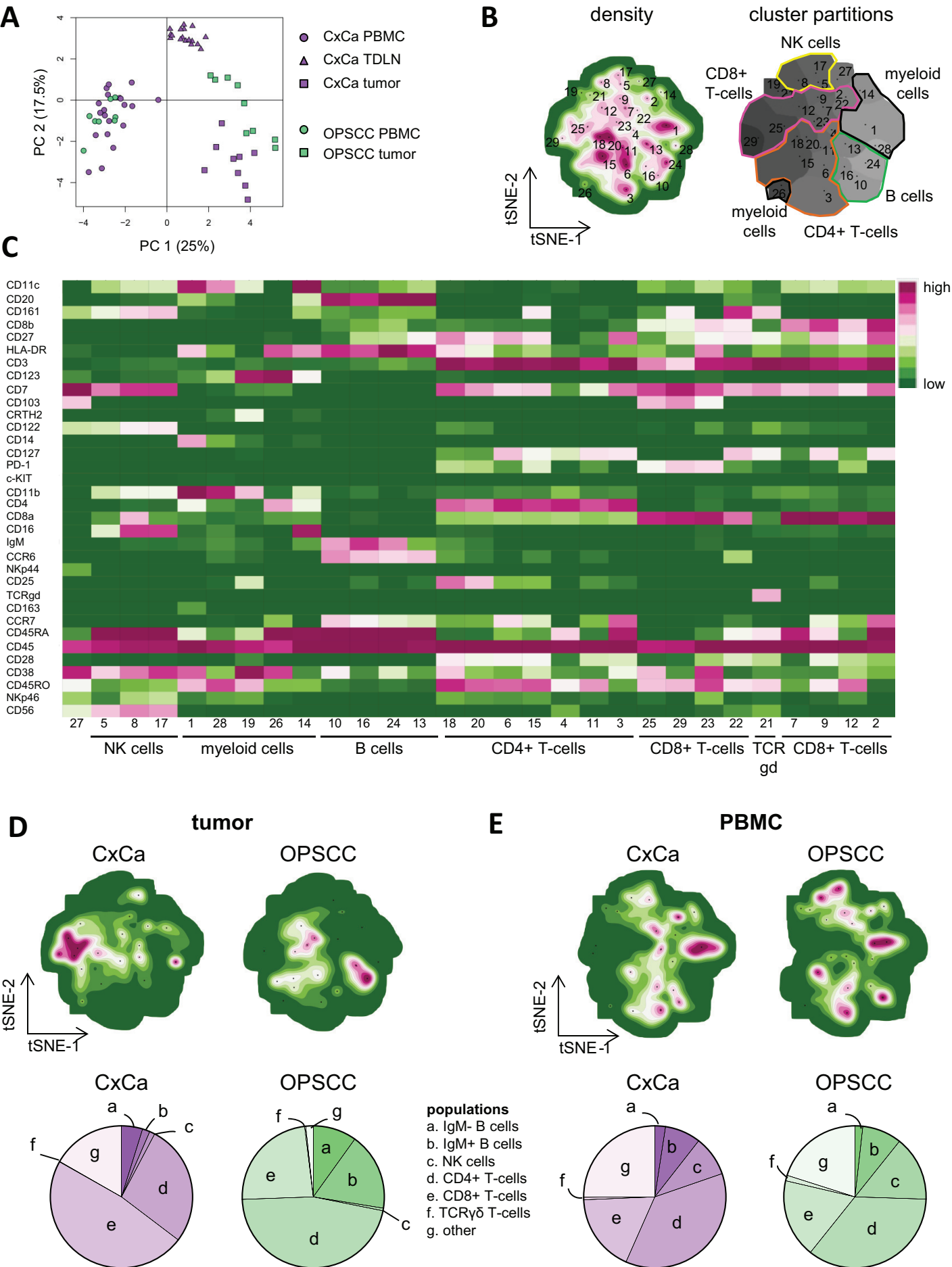
samples. (B and C) The distribution of naïve (Tn: CCR7+CD45RA+), central memory (Tcm: CCR7+CD45RA-), effector memory (Tem; CCR7-CD45RA-) and effector memory CD45RA+ (Temra: CCR7-CD45RA+) cells within CD8+ (B) and CD4+ (C) T-cells are given for indicated samples of CxCa patients (left), OPSCC patients (middle) and normal cervical epithelium and healthy tonsil (right). * $p < 0.05$; ** $p < 0.01$, *** $p < 0.001$ and **** $p < 0.0001$.

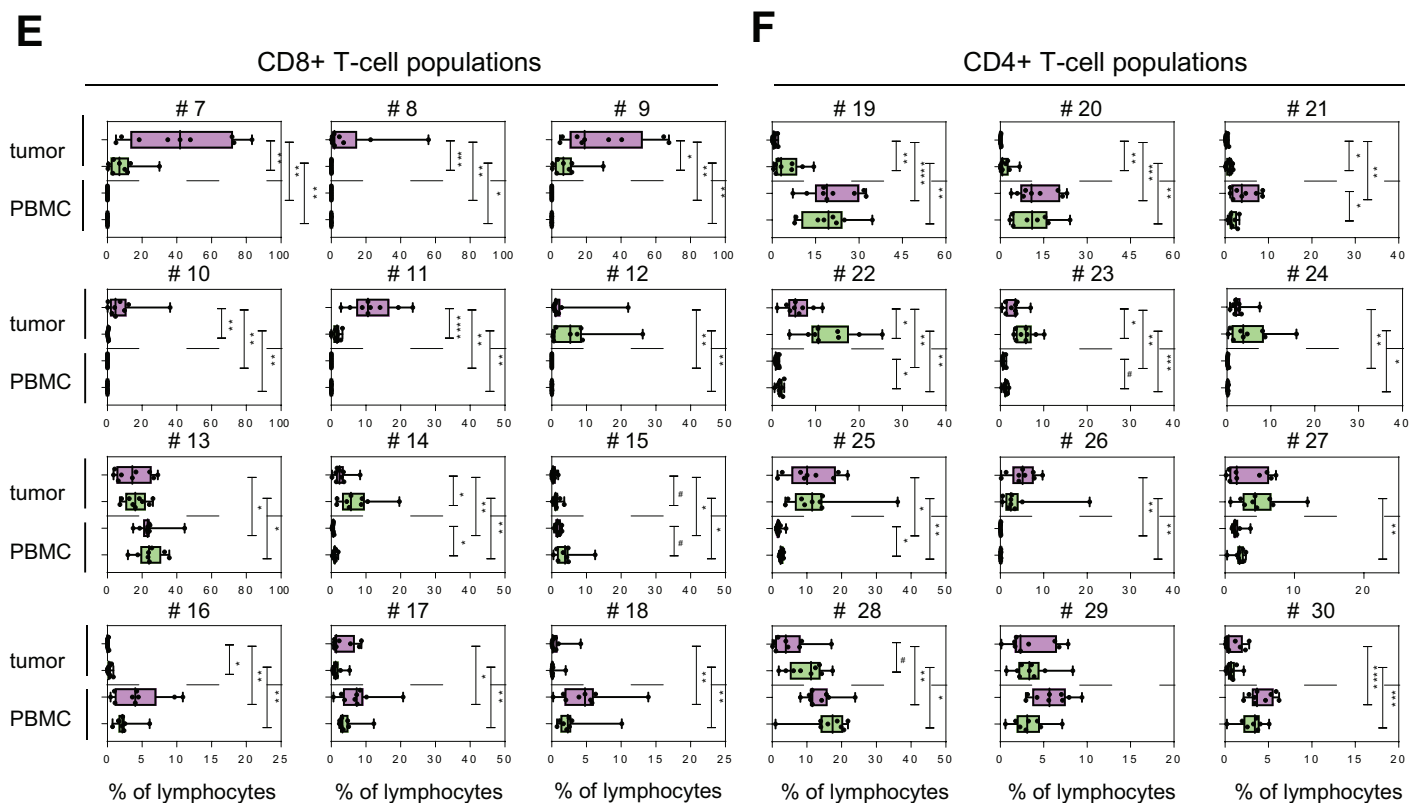
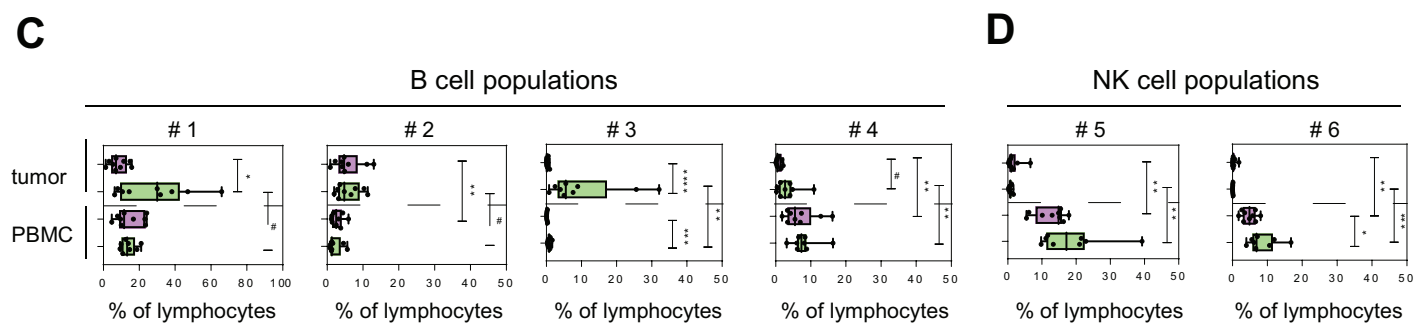
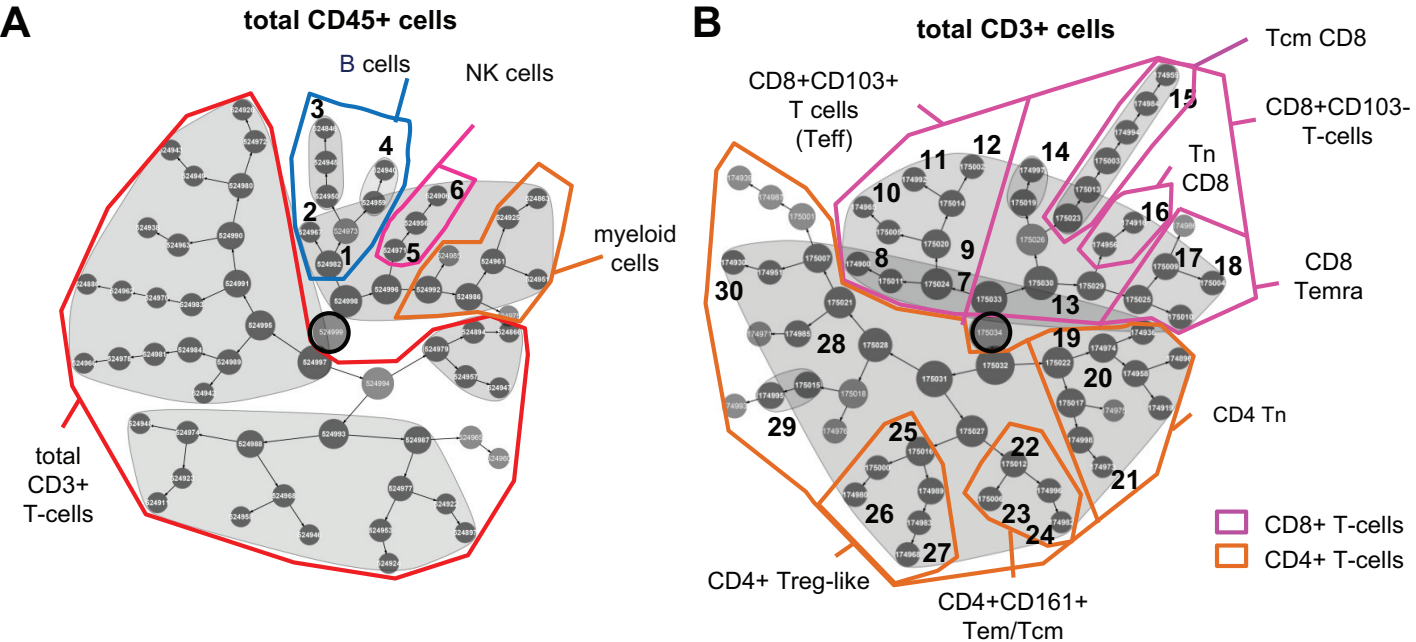
Figure 6. HPV16-specific T-cells are more frequently found in OPSCC and CxCa TDLN than CxCa. HPV16 specificity of tumor and LN-expanded T-cells was analyzed by 5-days [3H]-thymidine-based proliferation assay. Proliferation of tumor or LN-expanded T-cell cultures were tested in triplicate against autologous HPV16 E6/E7 peptide-loaded monocytes and CxCa and OPSCC tumors and LN were considered immune response positive (IR+) when the stimulation index (SI), calculated as the average proliferation of test wells divided by the average of the medium control wells, was > 3 . Depicted is the HPV16 IR status (IR+ or IR-) of 18 CxCa LN, 49 CxCa and 53 OPSCC samples. Statistical significance in HPV16-specific IR detection between CxCa LN, CxCa and OPSCC samples was calculated by two-tailed 2x3 Fisher exact probability test with Freeman-Halton extension. * $p < 0.05$; ** $p < 0.01$, *** $p < 0.001$ and **** $p < 0.0001$.

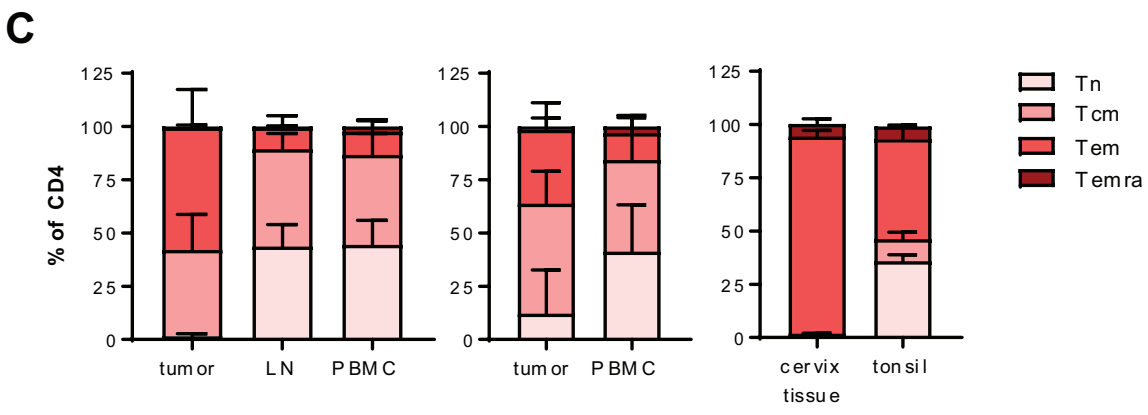
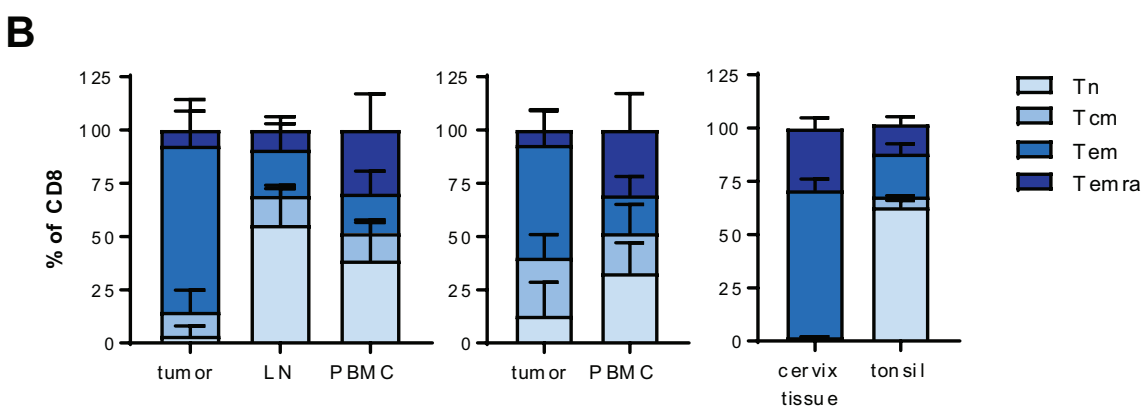
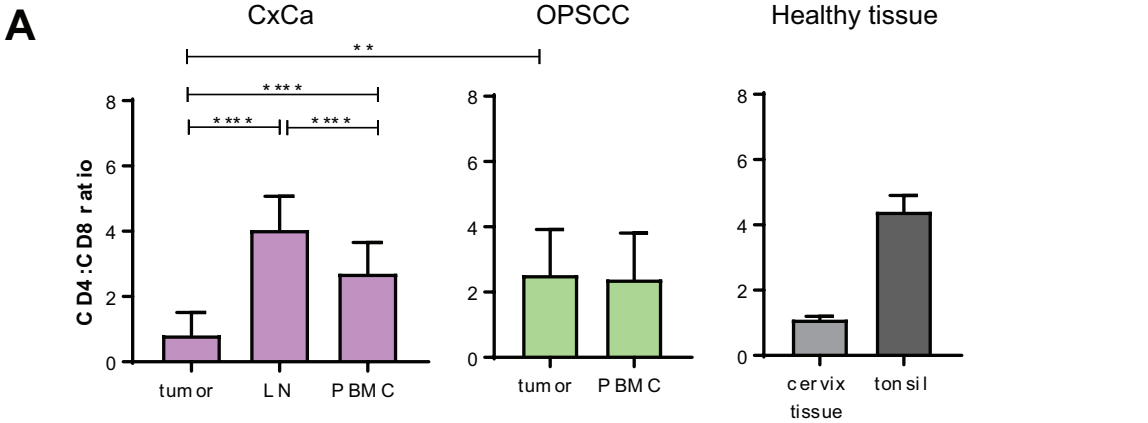
Figure 7. Differences in the magnitude of CD4+ T-cell infiltration between OPSCC and CxCa patients are reflected in their impact on survival. (A) Kaplan-Meier survival plots of 214 squamous CxCa patients in the TCGA database grouped according to high and low expression of CD4 (left), CD4 Tcm (middle) and CD4 Tem (right) in their tumor. (B) Kaplan-Meier survival plot of 38 HPV16/18+ CxCa patients from the LUMC from whom T-cell infiltration had been analyzed previously by us with immunohistochemistry (IHC) staining and were grouped on basis of the median number of tumor-infiltrating CD4 T-cells(28). (C and D) Kaplan-Meier survival curves showing the outcome of 42 tested HPV16-positive CxCa (c) and 51 HPV16-positive OPSCC patients (d) that were grouped based on the presence (immune response positive, IR+) or absence (immune response negative, IR-) of detectable HPV16-specific T-cells in their tumors. (E) Box and whiskers (plus min-max) plots displaying percentages of CD4+CD161+Tem (subset 22) detected in the tumor of HPV16 IR- and IR+

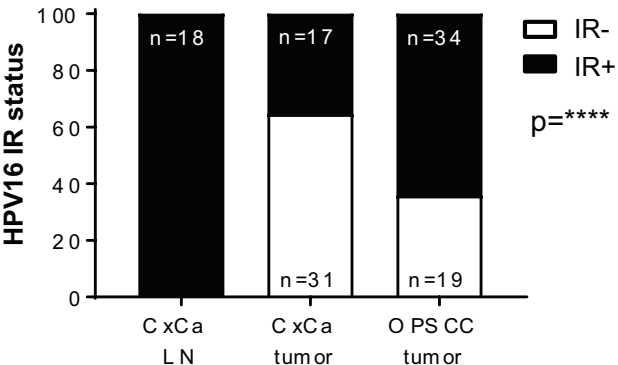
CxCa (purple) and OPSCC (green) patients. (F) Kaplan-Meier survival plots of 214 squamous CxCa patients in the TCGA database grouped according to high median expression of CD4 and CD161 (KLRB1) versus all others. For all Kaplan-Meier plots the hazard ratio (HR) with the 95% confidence interval (CI) as well as the log-rank test *P* value is given. NS, not significant; **p*<0.05; ***p*<0.01, ****p*<0.001 and *****p*<0.0001.

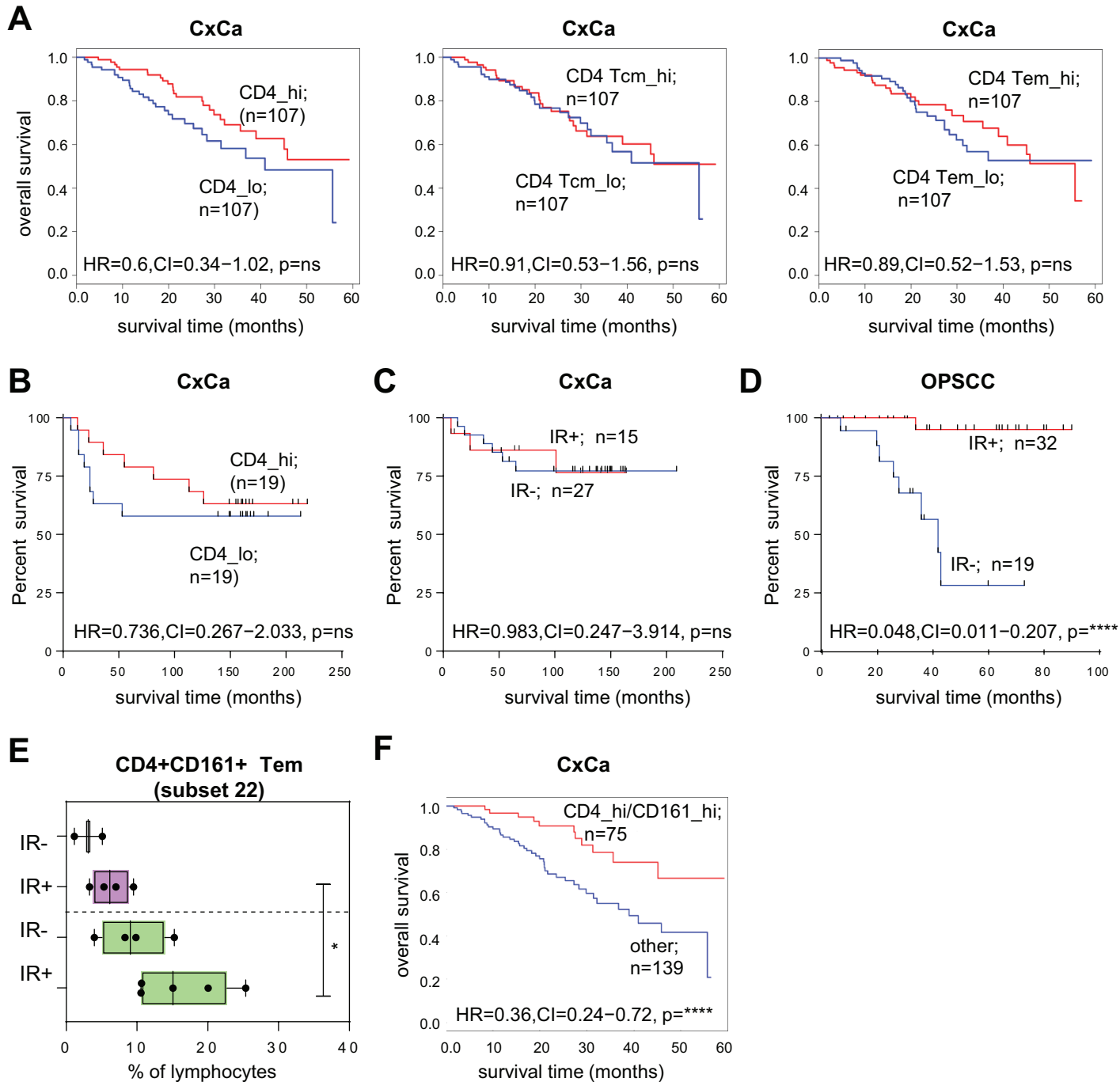












Clinical Cancer Research

The anatomical location shapes the immune infiltrate in tumors of same etiology and impacts survival

Saskia J Santegoets, Vanessa J van Ham, Ilina Ehsan, et al.

Clin Cancer Res Published OnlineFirst September 17, 2018.

Updated version	Access the most recent version of this article at: doi: 10.1158/1078-0432.CCR-18-1749
Supplementary Material	Access the most recent supplemental material at: http://clincancerres.aacrjournals.org/content/suppl/2018/09/15/1078-0432.CCR-18-1749.DC1
Author Manuscript	Author manuscripts have been peer reviewed and accepted for publication but have not yet been edited.

E-mail alerts	Sign up to receive free email-alerts related to this article or journal.
Reprints and Subscriptions	To order reprints of this article or to subscribe to the journal, contact the AACR Publications Department at pubs@aacr.org .
Permissions	To request permission to re-use all or part of this article, use this link http://clincancerres.aacrjournals.org/content/early/2018/09/15/1078-0432.CCR-18-1749 . Click on "Request Permissions" which will take you to the Copyright Clearance Center's (CCC) Rightslink site.